

Electrolyte gate dependent high-frequency measurement of graphene field-effect transistor for sensing applications

W. Fu,^{*} M. El Abbassi,[†] T. Hasler, M. Jung, M. Steinacher, M. Calame, and C. Schönenberger^{*}

Department of Physics, University of Basel, Basel, Switzerland and

[†]Ecole Normale Supérieure, International Center of Fundamental Physics, Paris, France

G. Puebla-Hellmann, S. Hellmüller, T. Ihn, and A. Wallraff

Department of Physics, ETH Zürich, Zürich, Switzerland

(Dated: August 27, 2018)

Abstract

We performed radiofrequency (RF) reflectometry measurements at 2–4 GHz on electrolyte-gated graphene field-effect transistors (GFETs) utilizing a tunable stub-matching circuit for impedance matching. We demonstrate that the gate voltage dependent RF resistivity of graphene can be deduced even in the presence of the electrolyte which is in direct contact with the graphene layer. The RF resistivity is found to be consistent with its DC counterpart in the full gate voltage range. Furthermore, in order to access the potential of high-frequency sensing for applications, we demonstrate time-dependent gating in solution with nanosecond time resolution.

PACS numbers: 73.61.Cw, 73.40.Mr

Owing to its atomically thin structure and exceptional high mobilities,¹⁻³ graphene is potentially well suited to radiofrequency (RF) applications. This prospect is reinforced by the relative openness of the RF-electronics industry to new materials without the requirement of a high on/off current ratio, which limits the application of graphene for digital applications.⁴ Much of the research conducted so far on graphene RF transistors has focused on the cut-off frequency, f_T , which is the highest frequency at which a field-effect transistor (FET) is useful in RF applications.⁵⁻¹⁰ For instance, graphene FETs (GFETs) with an intrinsic cut-off frequency of $f_T = 100 - 300$ GHz have been demonstrated,^{6,8} which are superior to the best silicon MOSFETs with similar gate lengths. Graphene full-wave rectification and consequently frequency conversion with high efficiency have also been demonstrated by making use of the ambipolar conduction properties.^{11,12} The cyclotron motion of the charge carriers of graphene in a magnetic field suggests further applications in non-reciprocal components.^{13,14} Moreover, the microwave properties of graphene antennas and transmission line have also been investigated.^{15,16}

Recently, there is also growing interest in applying graphene RF transistors to biochemical sensing applications.^{17,18} But in spite of the rapid advances in recent years, our understanding of the RF properties of graphene, especially with regards to sensing in a liquid environment, is still incomplete. Although it is known that atomically thin large area graphene behaves as a wideband resistor due to negligible skin effect and kinetic inductance,¹⁹ it is difficult to measure the device resistance directly at RF. This is due to the large shunt capacitance in conventional back or top-gated graphene RF transistors having a significant influence on the RF performance, hindering (if not preventing) the extraction of the intrinsic parameters of graphene.

In contrast to conventional oxide based back or top gating, electrolyte gating can be used to tune the properties of GFETs without shunting the propagating RF signal. This is because of the unique frequency dependent properties of the electrolyte. At DC and relatively low frequency $\lesssim 10$ MHz the ions in the electrolyte can instantly respond to potential changes. Due to ideal screening, an electrode in the electrolyte, even if placed far away from the graphene surface, is very strongly coupled to the graphene layer and therefore able to induce large changes in the carrier concentration in graphene. The typical Debye screening length in an ionic buffer solution at a concentration of 100 mM is as small as 1 nm. In contrast, at high frequency > 100 MHz the ions in the electrolyte start to lag behind the

AC electric field due to the viscosity of the solution.²¹ As a result, the electrolyte behaves as a pure dielectric at microwave frequency and the RF shunt gate capacitance is negligible considering that the physical gate electrode in the electrolyte can be placed far away from the graphene samples.

In this work, we explore the RF properties of electrolyte-gated GFETs by using an RF reflectometry technique. We demonstrated that it is possible to deduce the gate dependent RF resistivity of graphene at microwave frequencies by modeling the graphene sheet as an RC dissipative transmission line. The extracted RF resistivity of graphene is found to be consistent with its DC counterparts in the full gate voltage range. As a proof-of-principle for high-speed sensing applications in liquids, we demonstrate in addition nanosecond time-resolved measurements in electrolytes. We believe that this work opens the avenue for further research on a new generation of biochemical sensors. For example, owing to its wide bandwidth and significantly reduced $1/f$ noise at high frequencies, our graphene RF device will enable ultrafast measurements with a good detection limit, allowing to explore new phenomena and physics at the solid-liquid interface.

In reflectometry the intensity of the reflected wave of an RF signal is measured relative to the input signal yielding the frequency dependent reflection coefficient S_{11} . This value depends on the load impedance. The sensitivity to the load is optimized if the load impedance matches the characteristic impedance of the transmission line at $50\ \Omega$. In our graphene devices, typical resistances are in the range of $1 - 100\ \text{k}\Omega$, which is far off the matching value of the transmission line. To achieve a better signal, we use the recently developed approach^{22,23} based on stub-matching²⁴. Here, a stub is added to the waveguide to realize an impedance matching circuit that converts the large impedance of the graphene devices to a value close to $50\ \Omega$. The stub-matching circuit is realized on a printed circuit board (PCB, RO4003C) with coplanar waveguides (CPWs) and ground planes made from a $40\ \mu\text{m}$ Cu film with an additional $3 - 6\ \mu\text{m}$ Ni/ $0.1\ \mu\text{m}$ Au plating and integrated with the graphene sample, see Fig. 1. Reflectometry measurements are performed with a vector network analyzer (VNA) connected via a bias tee to the PCB. The bias tee is needed for DC measurements. All the components are placed at room temperature. Impedance matching is achieved by shunting the CPW connecting to the graphene sample by a stub placed at a distance of d_1 from the sample (Fig. 1b). The stub itself is a CPW with a length d_2 and is terminated by a varactor diode. The capacitance C_d of the diode can be tuned by applying a DC voltage V_d

through an additional on-chip bias tee as depicted in Fig. 1a and 1b (dashed red circle). To achieve impedance matching, both d_1 and d_2 have to be chosen close to $\lambda/4$, where λ is the wavelength of the 3 GHz carrier signal. The reflectometry setup is first calibrated up to the input of the PCB using standard procedures and commercial calibration kits. To calibrate the PCB board, frequency dependent measurements were performed with and without the graphene device.

Fig. 1c show the reflection coefficient S_{11} versus frequency f at different diode voltages V_d without a graphene device. First, by tuning the capacitance C_d of the diode, the best matching is achieved at around 3 GHz with $V_d = 8.72$ V (green line, Fig. 1c) where S_{11} is lower than -60 dB. At this resonant point at matching we measure a full width at half maximum of around 100 MHz, which places an upper limit on the setup bandwidth. Second, by fitting the frequency-dependent S_{11} curves using previously described calibration methods and models,^{22,23} we are able to extract the electrical lengths of $d_1 = 13.92$ mm and $d_2 = 14.12$ mm, values that are close to the design values $d_1 = 13.45$ mm and $d_2 = 13.75$ mm. The extracted attenuation constant of the CPW on the PCB is found to be $\alpha = 5.15$ dB/m at a frequency of 3 GHz, which is comparable to $\alpha \sim 4.6$ dB/m obtained from simulations of the PCB board (TXLINE 2003). After this calibration measurements, the graphene sample is glued into an 8×8 mm² recess at the end of the d_1 CPW and connected with several bonding wires at both sides. There are bonds from the d_1 stub to the graphene and on the opposite side a series of bonds to the ground plane. The graphene sample together with the bonding wires is then further encapsulated to allow for measurements in a liquid environment.

Previously, we have demonstrated that high-mobility GFETs with clean surfaces, and thus preserved chemical properties, can be fabricated using large-scale chemical vapor deposition (CVD).^{25,26} These transistors can serve as an ideal platform for biochemical sensing applications. In this study, we explore the microwave properties of such GFETs. As shown in Fig. 2a, we start with large area CVD graphene synthesized on Cu.²⁵⁻²⁷ Then a uniform layer of epoxy is put on a teflon substrate and a piece of graphene on copper is carefully placed over it upside down. The graphene flake is in direct contact with epoxy and on the opposite side the copper layer faces air. The edges of the Cu surface are then manually covered with PMMA as an easy way to obtain source and drain electrodes after etching the Cu film in the middle. Due to the good adhesion of the graphene flake on epoxy, the exposed Cu can be etched away in an ammonium persulfate solution leaving the intact graphene un-

derneath. Afterwards, the PMMA can be carefully peeled away to release the Cu electrodes. Such fabricated GFETs on teflon substrates are placed at the end of the stub tuner and connected with wire bonds. At the end of fabrication, an additional epoxy step is applied to seal the Cu electrodes as well as the bonding wires from liquid.

Fig. 2b shows the schematics and measurement circuits of such a GFET device. The electrostatic potential in the electrolyte is defined via a calomel reference electrode. This potential is gating the graphene sample. Fig. 2c shows the dependence of the measured DC electrical resistance R of a GFET as a function of the gate voltage applied to the calomel reference electrode V_{ref} (pink circle: forward, black star: backward sweep) in a 100 mM KCl solution. Negligible hysteresis can be identified in this transfer characteristics. This is an indication of the reliability and reproducibility of the device and the measurements.

After evaluating the DC transfer characteristics of the electrolyte-gated GFET, we measured its frequency dependent reflection coefficient S_{11} when sweeping the liquid gate voltage V_{ref} from -0.7 V to 0.1 V in steps of 0.1 V in 100 mM KCl solution. For reasons of clarity, Fig. 3a shows only a few curves measured at -0.7 V (green dots), -0.2 V (black dots), and 0.1 V (blue dots). In order to fit the measured curves, we introduce an RC dissipative transmission line model. This model treats the graphene sheet as a distributed RC line along which the RF signal propagates. We thereby neglect the graphene inductance which yields a negligible contribution to the impedance in our frequency range.¹⁹ Fig. 3a (inset) depicts such a circuit. Here, R' represents the resistance of graphene and C' the shunt capacitance both normalized per unit length. An RF wave propagating along the RC transmission line is damped due the resistive component. At a distance x , the amplitude of the RF signal will decrease by a factor of $\exp[-\sqrt{\omega R' C'} / 2x]$, where ω is the angular frequency. The characteristic propagation length over which the signal decays by a factor of $1/e$ is then given by $L_\lambda = \sqrt{2/\omega R' C'}$. The capacitance per unit length C' is determined by the dielectric materials leading to ground. As the ions in the liquid cannot follow the RF field at 3 GHz the main part of the capacitance is given by the substrate, and since the substrate capacitance is much smaller than the quantum capacitance C_Q ,²⁸ the latter does not play a role at RF frequencies. In order to keep this capacitance low enough we have chosen to work with teflon as a substrate material, hence, $C' = \varepsilon_o \varepsilon_{teflon} W/d$, with $d = 1$ mm the thickness of the teflon substrate and $W = 2.4$ mm the width of the graphene sheet. The water solution (electrolyte) on the upper surface yields only a secondary contribution to C' which is then

captured in the fitting by a slight increase in the effective dielectric constant relative to the published value of ε_{teflon} .

Having established a calibration up to the open end of the CPW, we need to also measure the contact resistance R_s and stray capacitance C_s of the bonding wires including the bonding pads. These values are obtained by fitting similar curves as in Fig. 3a after removal of the graphene in an O_2 plasma. Consequently, there are only two fitting parameters for each curve in Fig. 3, C' and R' . C' is related to an effective dielectric constant, while we convert R' into a sheet resistance or resistivity ρ given by $\rho = R'w$. The result of the fitting is shown in Fig. 3a as dashed curves. It turns out that all curves can be fitted with the same capacitance value C' . The extracted effective $\varepsilon_{teflon} = 2.4$ is found to be close to the reported dielectric constant of teflon which is 2.1. This strongly supports the proposed model. We stress here that this finding was reached by measurements carried out in both air and liquid environments at different salt concentrations and pH values (not shown).

The gate-dependent resistivity values ρ_{RF} deduced from the S_{11} measurements are shown together with the DC measurements ρ_{DC} in Fig. 3b. As can be seen, there is a perfect match between ρ_{RF} and ρ_{DC} . This is in agreement with the notion that the skin effect is negligible in ultra thin monolayer graphene.^{16,19} The graphene RF resistivity ρ_{RF} ranges between 1 and 5 k Ω , yielding a range of 0.4 to 2 k Ω /mm for R' . The shunting capacitance per area $C_{\square} = \varepsilon_o\varepsilon_{teflon}/d \sim 2 \times 10^{-8}$ F/m² yields $C' = 0.5$ aF/mm. This predicts a propagation length $L_{\lambda} \sim 1 - 2.3$ mm at 3 GHz, which is rather short. When the graphene sheet is longer than 1 mm, which is the case in the above device, the RF wave cannot propagate to the end, but most of the signal is dissipated before. We therefore stress that it is important to use a transmission line model and not only a fixed two-terminal graphene resistance. The latter parameter can be measured at low frequency. At high frequency the the resistivity is the more natural physical quantity.

Having demonstrated the ability to measure the gate-dependence of the graphene resistivity in an electrolyte, one may wonder how large the attainable measurement bandwidth is. We therefore performed time resolved measurements on the electrolyte-gated GFETs. The used homodyne measurement setup is sketched in Fig. 4a. A square wave at 2 MHz with a rise time of 7 ns is generated by a pulse generator and applied to the electrolyte gate of the GFET via a Au wire. The peak-to-peak voltage of the square wave is 200 mV and its low level is adjusted to the V_{CNP} of the GFET. At the same time, a -30 dBm RF

carrier signal (here at 3.55 GHz) is applied to the input of the stub tuner/GFET device via a directional coupler (-20 dB coupling). The resulting reflected signal exits the output port of the directional coupler and is down-converted to DC using a mixer with the carrier signal as local oscillator. Afterwards the signal is low pass filtered, amplified and recorded by an oscilloscope at a sampling rate of 1 GHz. Fig. 4b depicts the reference square wave (applied to the electrolyte gate via a Au wire) and the collected reflected signals for different KCl concentrations ranging from 1 mM to 1 M. We measure a rise time of $t_{rise} = 50$ ns in KCl solution for both 100 mM and 1 M concentrations. In contrast, in case of the 10 mM KCl solution the reflected signal starts to show a significant delay compared to the 2 MHz square wave. At even lower concentration of 1 mM concentration, the reflected signal is small and cannot build up on this time scale. Additional measurements reveal rise times of about $0.4 \mu\text{s}$ and $4 \mu\text{s}$ for a 10 mM and a 1 mM concentrated solutions.

The rise time is plotted in the inset of Fig. 4b as a function of ion concentration c . It can be quantitatively explained by looking into the equivalent RC circuits of the electrolyte-gated GFETs, which consists of the interfacial capacitance C_I and the series resistances to which both the water solution and graphene device contribute. First, the DC (or low frequency) interfacial capacitance C_I of an electrolyte-gated GFET can be modeled as two capacitors in series.^{26,28} One part is the quantum capacitance of graphene, C_Q , which is gate voltage dependent and has its minimum value at the charge neutral point (CNP). The other part is the double layer capacitance, C_{DL} , which is independent to the gate voltage. Here, in our case of moderate to high ionic strength (from 1 mM to 1 M), the double layer capacitance C_{DL} is limited by the Stern layer capacitance C_{Stern} which is on the order of 0.2 F/m^2 . This number is over one order of magnitude larger than the quantum capacitance of graphene $C_Q \sim 0.01 \text{ F/m}^2$ near the CNP at low carrier density. Hence, C_Q dominates the interface capacitance in the low frequency regime.^{26,28} Secondly, the resistance between the water solution and the graphene flake is inversely proportional to the KCl concentration, $R_W \propto 1/c$. It can be estimated to be about $10 \text{ k}\Omega$ to $10 \text{ M}\Omega$ for KCl concentrations in the range of 1 mM to 1 M. As a comparison, the resistance of our graphene flake is of the order of $\text{k}\Omega$. This is up four to orders of magnitude lower than that of the water solution R_W . Based on this discussion, the time constant of the system can be estimated as $\tau = R_W C_Q \propto 1/c$. This trend satisfactorily explains the observed KCl concentration dependent rise times of the electrolyte-gated GFET system seen in the inset of Fig. 4 (grey line). A saturation of the time scale occurs at ~ 50 ns

for large ion concentrations. This is an extrinsic effect mainly caused by the amplifier which (only) had a 10 MHz bandwidth, limiting the response to 35 ns. The linear dependence shows, however, that a 10 ns response time is feasible in a highly concentrated buffer solution as used in biological studies. This time scale would then also approach the bandwidth limit of the impedance matching circuit. The presented measurements demonstrate the feasibility of achieving nanosecond time resolution in measurements of the electrostatic potentials at the electrolyte graphene surface.

In conclusion, this work represents a systematic study of the gate voltage dependent characterization of large scale monolayer CVD GFET at microwave frequencies in a liquid environment. Using the reflectometry technique, we measured the frequency dependent reflection coefficient S_{11} at different electrolyte gate voltages. An RC dissipative transmission line model is proposed to extract the RF resistivity of GFETs after de-embedding, which is found to follow its DC counterparts. The tunable transmission lines realized by using high-mobility liquid-gated GFETs can serve as a platform for a new generation of biochemical sensors. Potentially, the wide bandwidth (100 MHz) offered by this high-frequency measurements enables ultra fast measurements in liquid with 10 ns time resolution.

Acknowledgments

The authors acknowledge funding from the Swiss Nanoscience Institute (SNI), Swiss National Science Foundation, nanotera.ch, NCCR-QSIT, ERC project QUEST, FP7 projects Symone and Graphene Flagship. W. Fu and M. El Abbassi contributed equally to this work.

* Electronic address: Wangyang.Fu@unibas.ch; Christian.Schoenenberger@unibas.ch

¹ K. S. Novoselov, A. K. Geim, S. V. Morozov, D. Jiang, Y. Zhang, S. V. Dubonos, I. V. Grigorieva, A. A. Girsov, Electric field effect in atomically thin carbon films. *Science* **2004**, *306*, 666-669.

² K. S. Novoselov, D. Jiang, F. Schedin, T. J. Booth, V. V. Khotkevich, S. V. Morozov, A. K. Geim, Two-dimensional atomic crystals. *Proc. Natl. Acad. Sci. U. S. A.* **2005**, *102*, 10451-10453.

³ S. Das Sarma, S. Adam, E. H. Hwang, E. Rossi, Electronic transport in two dimensional graphene. *Rev. Mod. Phys.* **2011**, *83*, 407-470.

- ⁴ Frank schwierz, Graphene transistors. *Nat. Nanotech.* **2010**, 5, 487-496.
- ⁵ Y. M. Lin, H. Y. Chiu, K. A. Jenkins, D. B. Farmer, Ph. Avouris, A. Valdes-Garcia, Dual-gate graphene FETs with f_T of 50 GHz. *IEEE Electron Device Lett.* **2010**, 31, 68C70.
- ⁶ Y. M. Lin, C. Dimitrakopoulos, K. A. Jenkins, D. B. Farmer, H.-Y. Chiu, A. Grill, Ph. Avouris, 100-GHz transistors from wafer-scale epitaxial graphene. *Science* **2010**, 327, 662.
- ⁷ E. Pallecchi, C. Benz, A. C. Betz, H. v. Löhneysen, B. Plaçais, R. Danneau, Graphene microwave transistors on sapphire substrates. *Appl. Phys. Lett.* **2011**, 99, 113502.
- ⁸ L. Liao, Y. C. Lin, M. Bao, R. Cheng, J. Bai, Y. Liu, Y. Qu, K. L. Wang, Y. Huang, X. Duan, High-speed graphene transistors with a self-aligned nanowire gate. *Nature* **2010**, 467, 305-308.
- ⁹ C. R. Dean, A. F. Young, I. Meric, C. Lee, L. Wang, S. Sorgenfrei, K. Watanabe, T. Taniguchi, P. Kim, K. L. Shepard, J. Hone, Boron nitride substrates for high-quality graphene electronics. *Nat. Nanotech.* **2010**, 5, 722-726.
- ¹⁰ H. Wang, T. Taychatanapat, A. Hsu, K. Watanabe, T. Taniguchi, P. Jarillo-Herrero, T. Palacios, BN/graphene/BN transistors for RF applications, *IEEE Electron Device Lett.* **2011**, 32, 1209-1211.
- ¹¹ H. Wang, D. Nezich, J. Kong, T. Palacios, Graphene frequency multipliers. *IEEE Electron Device Lett.* **2009**, 30, 547-549.
- ¹² Z. Wang, Z. Zhang, H. Xu, L. Ding, S. Wang, L. M. Peng, A high-performance top-gate graphene field-effect transistor based frequency doubler. *Appl. Phys. Lett.* **2010**, 96, 173104.
- ¹³ D. L. Sounas and C. Caloz, Electromagnetic nonreciprocity and gyrotropy of graphene. *Appl. Phys. Lett.* **2011**, 98, 021911.
- ¹⁴ A. Fallahi and J. Perruisseau-Carrier, Manipulation of giant faraday rotation in graphene meta-surfaces *Appl. Phys. Lett.* **2012**, 101, 231605.
- ¹⁵ J. Perruisseau-Carrier, Graphene for antenna applications: opportunities and challenges from microwaves to THz. *arXiv:1210.3444* (2012).
- ¹⁶ M. Dragoman, D. Neculoiu, A. Cismaru, A. A. Muller, G. Deligeorgis, G. Konstantinidis, D. Dragoman, R. Plana, Coplanar waveguide on graphene in the range 40 MHz–110 GHz. *Appl. Phys. Lett.* **2011**, 99, 033112.
- ¹⁷ I. Iramnaaza, Y. Xinga, K. Xuea, Y. Zhuanga, R. Fitchb, Graphene based RF/microwave impedance sensing of DNA. *Electronic Components and Technology Conference (ECTC), 2011 IEEE 61st* **2011**, 1030-1034.

- ¹⁸ T. Le, T. Thai, V. Lakafosis, M. Tentzeris, Z. Lin, Y. Fang, K. Sandhage, C. Wong, Graphene enhanced wireless sensors. *Sensors, 2012 IEEE* **2012**, 1-4.
- ¹⁹ H. S. Skulason, H. V. Nguyen, A. Guermoune, V. Sridharan, M. Siaj, C. Caloz, T. Szkopek, 110 GHz measurement of large-area graphene integrated in low-loss microwave structures. *Appl. Phys. Lett.* **2011**, *99*, 153504.
- ²⁰ S. Kim, J. Nah, I. Jo, D. Shahrjerdi, L. Colombo, Z. Yao, E. Tutuc, S. K. Banerjee, Realization of a high mobility dual-gated graphene field-effect transistor with Al₂O₃ dielectric. *Appl. Phys. Lett.* **2009**, *94*, 062107.
- ²¹ J. O'M. Bockris, E. Gileadi, K. Müller, Dielectric Relaxation in the Electric Double Layer. *J. Chem. Phys.* **1966**, *44*, 1445.
- ²² S. Hellmüller, M. Pikulski, T. Müller, B. Küng, G. Puebla-Hellmann, A. Wallraff, M. Beck, K. Ensslin, T. Ihn, Optimization of sample-chip design for stub-matched radio-frequency reflectometry measurements. *Appl. Phys. Lett.* **2012**, *101*, 042112.
- ²³ G. Puebla-Hellmann and A. Wallraff, Realization of gigahertz-frequency impedance matching circuits for nanoscale devices. *Appl. Phys. Lett.* **2012**, *101*, 053108.
- ²⁴ D. M. Pozar, Microwave engineering. *John Wiley & Sons, Inc., United States of America* **2005**, 3rd ed.
- ²⁵ W. Fu, C. Nef, O. Knopfmacher, A. Tarasov, M. Weiss, M. Calame, C. Schönenberger, Graphene Transistors Are Insensitive to pH Changes in Solution. *Nano Lett.* **2011**, *11*, 3597-3600.
- ²⁶ W. Fu, C. Nef, A. Tarasov, M. Wipf, R. Stoop, O. Knopfmacher, M. Weiss, M. Calame, C. Schönenberger, High mobility graphene ion-sensitive field-effect transistors by noncovalent functionalization. *submitted* **2013**.
- ²⁷ X. S. Li, W. W. Cai, J. An, S. Kim, J. Nah, D. X. Yang, R. Piner, A. Velamakanni, I. Jung, E. Tutuc, S. K. Banerjee, L. Colombo, R. S. Ruoff, Large-area synthesis of high-quality and uniform graphene films on copper foils. *Science* **2009**, *324*, 1312-1314.
- ²⁸ J. Xia, F. Chen, J. Li, N. Tao, Measurement of the quantum capacitance of graphene. *Nat. Nanotech.* **2009**, *4*, 505-509.
- ²⁹ G. S. Kulkarni and Z. Zhong, Detection beyond the Debye screening length in a high-frequency nanoelectronic biosensor. *Nano Lett.* **2012**, *12*, 719-723.

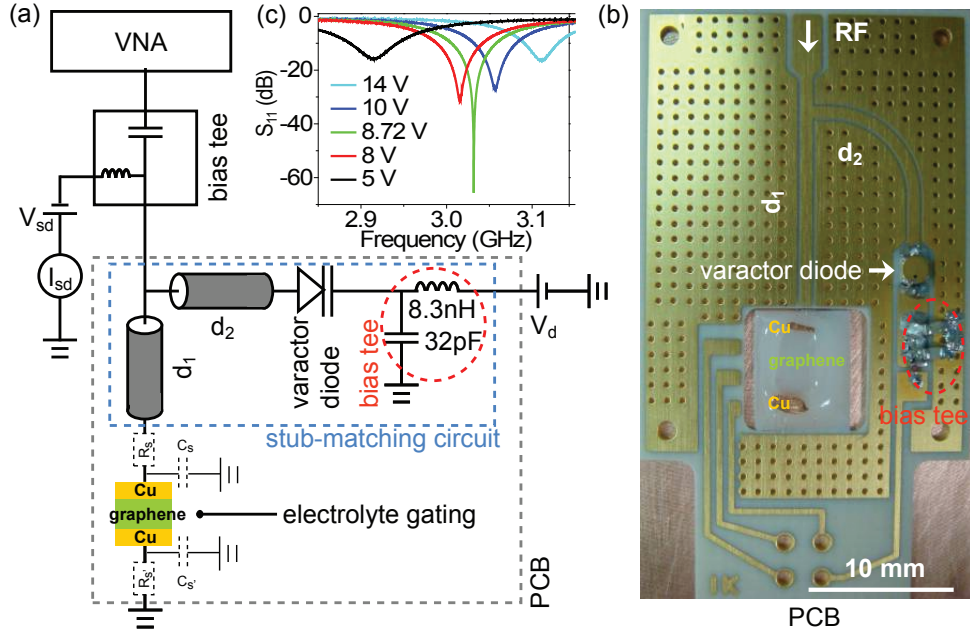


FIG. 1: (a) Experimental setup used to perform the reflectometry measurements at carrier frequencies of 2-4 GHz. (b) A picture of the PCB with a terminated waveguide (d_1) and a shunted stub (d_2). The graphene sample is connected to the d_1 waveguide via wire bonding and d_2 stub is terminated by a varactor diode, after which two capacitors and one inductor are placed as on-chip bias tee. (c) Open loop reflection coefficient S_{11} as a function of the carrier frequency f measured under different varactor diode bias voltages V_d .

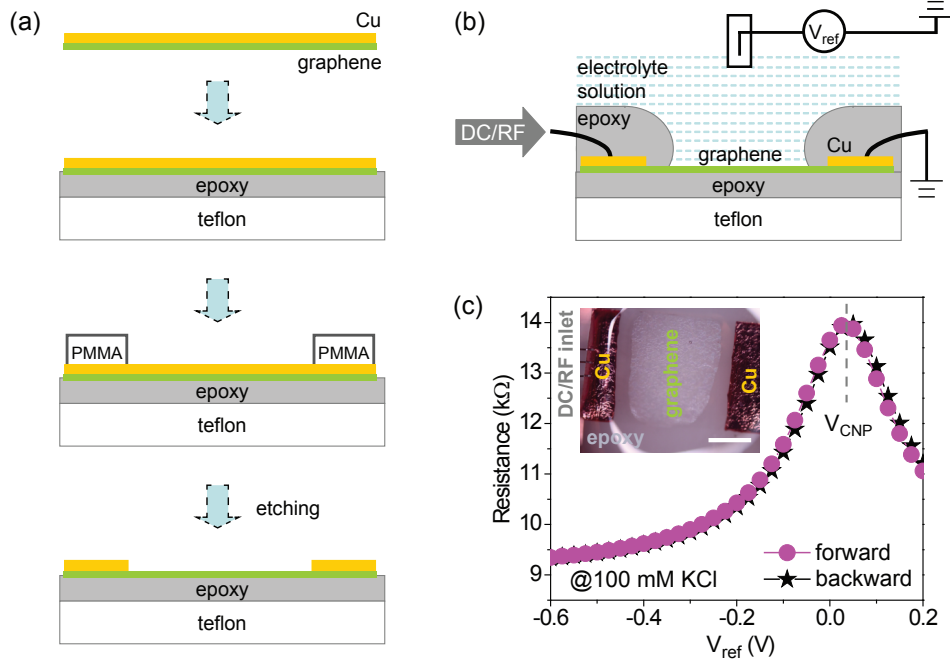


FIG. 2: GFET fabrication and measurement scheme. (a) Process flow for transferring and patterning a CVD graphene sheet (green) with clean surface. (b) Schematic of a fabricated GFET with liquid sealing and the electrical circuitry of the electrolyte-gated GFET. The electrostatic potential in the solution was defined by a commercial calomel reference electrode as V_{ref} or by a Au wire. (c) Electrical resistance of a GFET as a function of the reference potential V_{ref} measured in 100 mM KCl solution with negligible hysteresis. Inset, an optical image of the GFET under test. Scale bar: 1 mm.

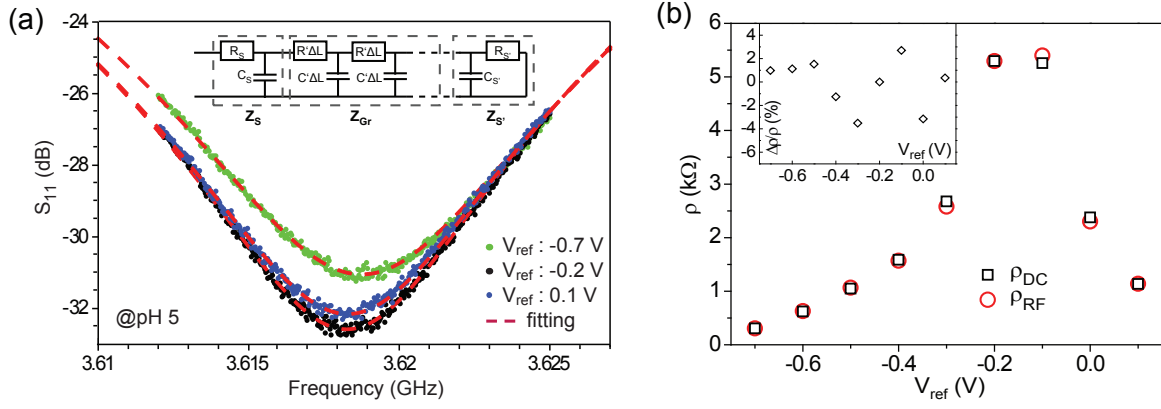


FIG. 3: (a) The measured reflection spectra at different liquid gate voltages V_{ref} and the corresponding fitting curves. Inset: the RC dissipative transmission line model. (b) The measured DC resistivity ρ_{DC} (black squares) and the extracted small-signal RF resistance ρ_{RF} (red circles) as a function of the applied liquid gate voltage V_{ref} . Inset: the relative deviation between ρ_{DC} and ρ_{RF} ($\Delta\rho/\rho := (\rho_{RF} - \rho_{DC})/\rho_{DC} \times 100\%$) as a function of the applied liquid gate voltage V_{ref} .

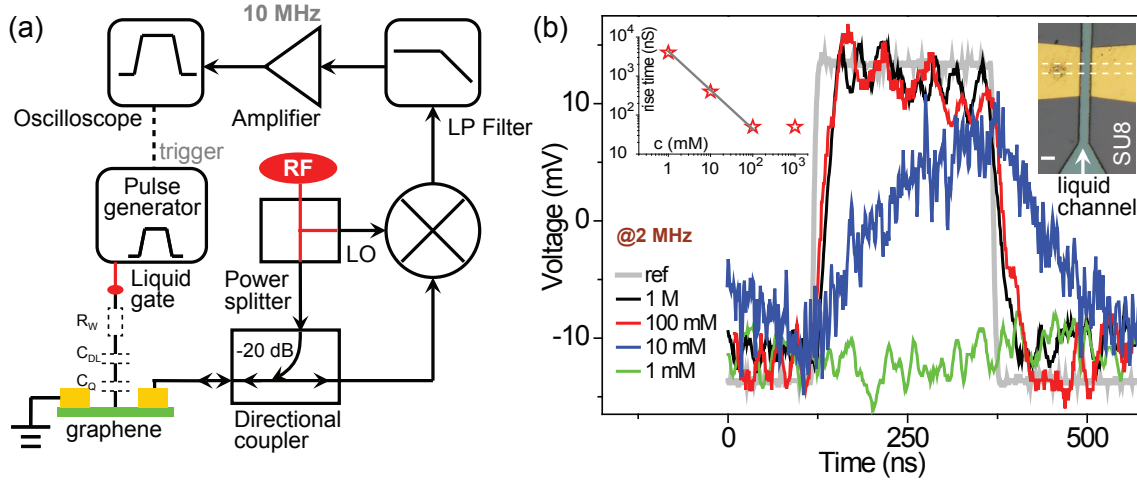


FIG. 4: (a) Schematic of the time-resolved homodyne measurement setup. (b) Sensing responses of the GFET to a 500 ns square wave reference signal with 200 mV peak-to-peak voltage applied to the liquid gate (normalized, grey line), in KCl solutions with concentration of 1 mM (green line), 10 mM (blue line), 100 mM (red line) and 1 M (black line). Inset, to the right: an optical image of the GFET with SU-8 (a photoresist) liquid sealing. The dashed white line is an indication of the graphene ribbon. Scale bar: 10 μm . To the left: measured rise times as a function of the KCl concentration c . The grey line indicates a linear $1/c$ behavior.